

# Analysing immune cell migration

Joost B. Beltman\*, Athanasius F. M. Marée† and Rob J. de Boer\*

**Abstract** | The visualization of the dynamic behaviour of and interactions between immune cells using time-lapse video microscopy has an important role in modern immunology. To draw robust conclusions, quantification of such cell migration is required. However, imaging experiments are associated with various artefacts that can affect the estimated positions of the immune cells under analysis, which form the basis of any subsequent analysis. Here, we describe potential artefacts that could affect the interpretation of data sets on immune cell migration. We propose how these errors can be recognized and corrected, and suggest ways to prevent the data analysis itself leading to biased results.

## Time-lapse video microscopy

A microscopy technique in which sequential static images from multiple time frames are combined into a video displayed at a faster rate than the images were acquired.

## Two-photon excitation

A technique by which fluorescent markers are excited by the nearly simultaneous absorption of two photons of low energy, resulting in the emission of fluorescent light that is collected by a detector.

## Image volume

The three-dimensional volume, typically in the shape of a box, from which emitted fluorescence, and thus fluorescently labelled cells, can be detected.

Since the beginning of the twenty-first century it has been possible to visualize the dynamic behaviour of immune cells in living lymphoid tissues using time-lapse video microscopy<sup>1–6</sup>, whereby fluorescently labelled cells are usually visualized by two-photon excitation. This has resulted in spectacular videos of the *in vivo* behaviour of, and interactions between, various types of immune cell. Robust conclusions from such data require detailed quantitative analysis of the position and movement of cells, particularly to detect subtle cell migration phenomena. Time-lapse imaging experiments are complicated to carry out, and the tracking of cell movement from the resulting videos is a laborious and error-prone process. In this Review, we discuss artefacts that are expected to be present in imaging data sets and explain how these can influence the obtained results. We propose how data analysis can assist in the detection as well as correction of these artefacts. We start by reviewing frequently used parameters for analysing cellular motility. Then we provide an overview of potential artefacts in data sets, as well as other problems associated with the analysis of cell migration and interactions, and suggest solutions for these issues.

## Overview of common motility parameters

Several motility parameters are frequently used to quantitate cell migration behaviour. Such analysis starts after the experiments and cell tracking have been carried out, so at each time point the location of all cells has been estimated.

**Plotting tracks.** By plotting the trajectories of the tracked centres of mass of immune cells over time in two or three dimensions, the migratory behaviour of the cell population can be qualitatively examined. One option is to simply plot the unshifted coordinates of the centres of mass in the image volume, possibly overlaid on the acquired

images of the cells. This can help to see whether the visualized cells prefer particular regions of the tissue. This approach has recently been used to show that mutations in signalling lymphocyte activation molecule-associated protein (SAP; also known as SH2D1A) cause follicular T helper cells to be largely excluded from germinal centres and instead reside mainly in the follicular mantle of B cell regions<sup>7</sup>.

The other option is to shift the starting position of each individual cell to the same point in space while maintaining its orientation (FIG. 1a), allowing one to roughly see whether cells are travelling in a preferred direction. If all possible directions of migration are approximately equally covered, this indicates that motion is more or less random on the timescale of the duration of the plotted tracks. However, plotting tracks only gives a qualitative indication of cell movement.

**Speed.** One of the most frequently studied migration parameters is cell migration speed, and an early finding of two-photon imaging of lymph nodes was that T cells are activated in several phases that differ in migration parameters such as speed<sup>5,8</sup>. The mean speed over the brief interval between two sequential time frames can be approximated by dividing the distance the cell travels by the time period between the frames. Because in reality a trajectory will not be exactly straight, this is an underestimate of the true speed of the cell. The longer the time period between the frames, the larger this error will be. However, this error remains limited provided that the time period between frames is shorter than the time period for which cells tend to move in a persistent direction. A frequently used parameter that is derived from speed is the arrest coefficient, which is the fraction of time that a cell is ‘pausing’ (usually defined as having a speed less than 2  $\mu\text{m}$  per minute).

\*Theoretical Biology, Utrecht University, Padualaan 8, 3584 CH Utrecht, The Netherlands.

†John Innes Centre, Norwich Research park, Colney, Norwich, NR4 7UH, UK. Correspondence to J.B.B. e-mail: J.B.Beltman@uu.nl doi:10.1038/nri2638

Published online 16 October 2009

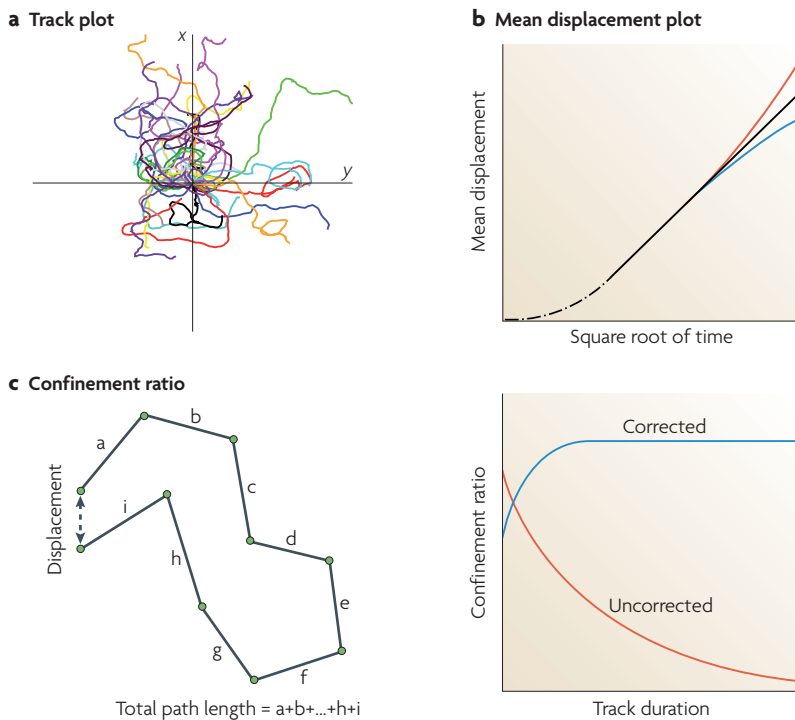


**Figure 1 | Commonly calculated migration parameters.** **a** | A track plot in which each track has been shifted such that it starts at the origin of the x and y axes. **b** | Plotting the mean displacement of cells against the square root of time gives information about the type of migration involved. A linear relationship is indicative of random walk (straight black line). Over short timescales, cells typically displace faster than random, which is termed persistent motion (dash-dotted black line). When this occurs over long timescales it provides evidence for directional migration (red line), whereas a slower than linear increase in the mean displacement denotes confined migration (blue line). **c** | The confinement ratio is calculated by dividing the displacement of the cell by its total path length. In the 'corrected' confinement ratio the resulting value is multiplied by the square root of the cell track duration. The right panel shows how the confinement ratio and its corrected version depend on the track duration. The uncorrected ratio tends to zero for large track durations, whereas the corrected ratio reaches a constant number (for random migration).

**Mean displacement.** To determine the type of locomotion of the visualized cell population, researchers frequently analyse how the mean displacement of cells depends on the time period for which the cells are followed. The displacement of a cell is the shortest distance between the positions at two time points (which is distinct from the length of the entire path it has travelled). Typical cell motility can be deduced from a plot of the mean displacement versus the square root of time (FIG. 1b). If this relationship is linear, it means that cells behave as randomly moving objects, and a motility coefficient can be calculated (see example in REF. 9). However, published values of motility coefficients are typically underestimated because a correction is required when the mean displacement rather than the mean of the squared displacements is used in the calculations (see [Supplementary information S1](#) (box) and REF. 10).

A faster than linear increase in the mean displacement plot is reminiscent of directed motion. Cells exhibit directed motion for typically at least a few minutes, which means that on short timescales they

tend to move in an approximately straight line (in a persistent direction). When such directed motion is also observed on long timescales this means that the cells displace more than expected for a random walk. One factor that could cause directed motion is if the immune cells were to follow a chemokine gradient. A slower than linear increase of the mean displacement plot means that the cells are somehow confined, for example because interactions with other cell types keep them within a specific region. It was recently suggested that thymocytes exhibit such confined behaviour during negative selection in the medulla, but not in the cortex, of the thymus<sup>11</sup>.

Although the mean displacement plot is a useful tool to investigate the type of motility involved, the underlying mechanism of migration cannot be inferred from it. This is because multiple underlying micro-processes can give rise to the same or very similar mean displacement plots<sup>12-14</sup>. For example, viewing the migration of T cells in lymph nodes as consisting of randomly oriented steps of fixed duration and speed<sup>10</sup> or as persistently moving cells that manoeuvre through a densely packed organ with highly variable speeds<sup>15</sup> results in similar mean displacement plots.

**Confinement ratio.** Sometimes researchers are interested in calculating a parameter known as the confinement ratio (also known as the chemotactic index, meandering index or straightness index)<sup>16,17</sup>. This is a measure of the straightness or confinement of cell tracks, and it is the ratio of the displacement of a cell to the total length of the path that the cell has travelled (FIG. 1c). Because the path length is always at least the distance of the displacement, the confinement ratio can vary between 0 (a completely condensed cell track, so the cell returns to the exact position where it started) and 1 (a perfectly straight cell track). For example, the role of CD44, a receptor for extracellular matrix proteins and glycosaminoglycans, was investigated in the migration of cytotoxic T lymphocytes in tumours using a combination of cell speed and confinement ratio to quantify various behaviours among these lymphocytes<sup>18</sup>.

A problem with the confinement ratio is that its value tends to zero as the track duration goes to infinity (FIG. 1c uncorrected ratio; see also REFS 6 and 17, and [Supplementary information S2](#) (figure) for an example from an experimental data set). This can be seen by noting that the confinement ratio is closely linked to a mean displacement analysis (see [Supplementary information S1](#) (box)). Thus, a comparison of cell tracks of different durations and of different experiments is problematic. One way to solve this is to calculate the confinement ratio for a certain duration, but this means discarding shorter cell tracks as well as parts of cell tracks that exceed the chosen duration. Another way to circumvent the problem of dependency on the cell track duration is to multiply the confinement ratio of a cell by the square root of time; this simple 'correction' removes the dependency on track duration (FIG. 1c, corrected ratio). To use this

**Motility coefficient**

A measure for how fast cells displace from their starting positions during a random walk process. It is identical to a diffusion coefficient.

**Persistent motion**

The phenomenon that cells generally travel in relatively straight lines on a short timescale (usually of minutes).

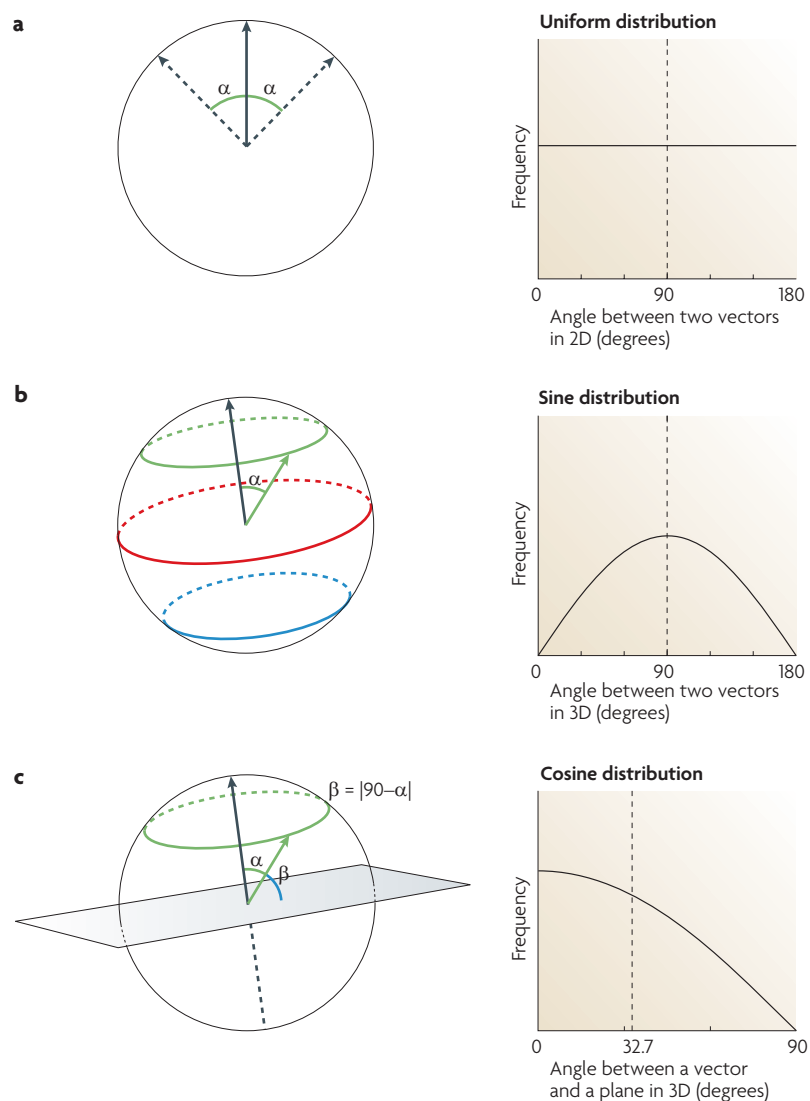


**Figure 2 | Angle distributions expected for random migration. a** | In two dimensions (2D) all possible unit vectors together form a circle. The angle between two vectors is denoted by  $\alpha$ . The frequency distribution of two vectors with random orientation in 2D is uniform as each of the angles has an equal probability of occurring. The mean is 90 degrees. **b** | In three dimensions (3D) all possible unit vectors map onto a sphere. For each of the coloured circles, the vectors that together compose that particular circle share the same angle to the black vector (example angle  $\alpha$  is shown for the green circle). The frequency distribution of angles between two vectors with random orientation in 3D follows a sine distribution because the size of each circle reflects the relative probability of occurrence of the associated migration angle. The mean is 90 degrees. **c** | The angle between a vector and a plane in three dimensions ( $\beta$ ) can be derived from the angle with the normal vector to the plane ( $\alpha$ ). The frequency distribution of angles between a plane and a vector with random orientation in 3D is a cosine distribution. The mean of a cosine distribution is  $\sim 32.7$  degrees ( $90 - (180 \div \pi)$ ).

**Migration angles.** In time-lapse imaging, a moving cell is observed by taking snapshots at constant time intervals, hence the motion of each cell is regarded as a sequence of vectors. Because these vectors have a direction associated with them, it is possible to calculate angles between the direction of migration and various other directions in space (such as the orientation of certain anatomical structures). The distribution of angles that can be expected for random migration differs for angles in two dimensions and three dimensions. If we draw all possible unit vectors in two dimensions, they map onto a circle (FIG. 2a). Because each point on the circle has an equal probability of occurring, the frequency distribution of angles between two random vectors becomes a uniform distribution.

When we draw all possible unit vectors in three dimensions, they map onto a sphere. If we subsequently split that sphere into differently sized circles in three-dimensional space, each circle then consists of a set of unit vectors that have a particular migration angle with a reference vector in common (FIG. 2b). The size of each circle reflects the relative probability of occurrence of the migration angle associated with that circle. The possible angles vary from 0 to 180 degrees but, contrary to the case for two dimensions, migration angles of around 90 degrees are most likely to occur in three dimensions, as these form the biggest circles. The frequency of angles between two random vectors follows a sine distribution<sup>19,20</sup>.

In addition to measuring the angle between two vectors, in three dimensions the angle between a vector and a plane can also be measured. The distribution expected in this case is most easily determined by defining the plane by its normal vector (that is, a vector perpendicular to the plane). The angle of a random vector to the plane can then be calculated from the angle of the random vector to the normal vector (FIG. 2c). The resulting distribution expected for random vectors becomes a cosine distribution. Possible angles in this cosine distribution vary from 0 to 90 degrees, where angles that are approximately parallel to the plane are the most likely to occur and angles that are orthogonal to the plane are the least likely.

By knowing the angle distribution expected for a cell migration process that is completely random, it is possible to compare observed and expected angle distributions to see whether there is a difference from random migration (for example, to see if it is directed migration). The expected means in the case of random migration are 90 degrees for the angle between two vectors in both two and three dimensions, and approximately 32.7 degrees for the angle between a vector and a plane in three dimensions.

There are many different settings where this method can be used. One frequently calculated angle is the observed turning angle of a cell between sequential time frames (FIG. 3a), which together with the cell speed gives information about how far cells can travel in a limited time period. Because cells generally move in a persistent direction at timescales of up to a few minutes, the distribution of turning angles is skewed to small values (FIG. 3b). The turning angle distribution depends on the time period between frames. A long time interval makes it

**Frequency distribution**  
Enumeration of all values that a variable can take and the relative number of times each value occurs.

approach to directly compare cell tracks of different durations, the total track duration should be longer than the typical duration of persistent motion, and the time interval between sequential images should be shorter than the typical duration of persistence (see Supplementary information S1 (box)). The disadvantage of this 'corrected' confinement ratio is that the values are not unitless and are not restricted to between 0 and 1.

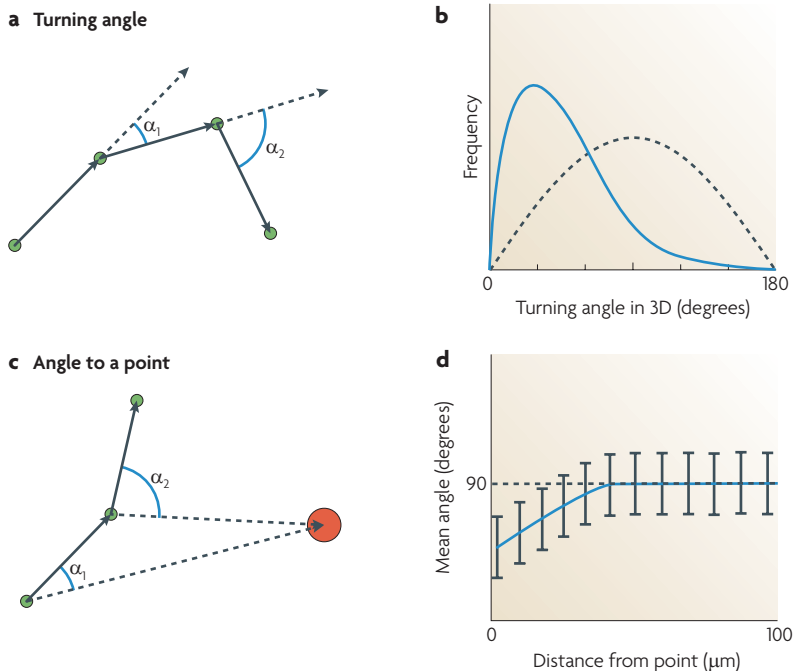


**Figure 3 | Examples of migration angles.** **a** | The turning angles a cell makes are the angles between sequential time points of imaging. Shown are examples of angles at two successive time points; solid arrows and green circles show the actual migration path, and dashed arrows project the previous migration directions, which are used to calculate the turning angles ( $\alpha_1$  and  $\alpha_2$ ). **b** | An example distribution of turning angles in three dimensions (3D). For random migration a sine distribution is expected (dotted line). However, turning angle distributions are typically skewed towards smaller angles (solid line) owing to persistent motion. **c** | The angle ( $\alpha_1$  or  $\alpha_2$ ) between the travel direction of a cell (green dots and solid arrows) and the shortest route (dashed arrows) towards a point of interest (red dot). **d** | A plot of the mean migration angle (and standard errors) between the direction of travel of a cell and the shortest route to a local point of interest against the distance to that position. If the mean is smaller than 90 degrees cell migration is directed towards the point of interest.

**Uniform distribution**

A distribution in which there is a defined maximum and minimum that a value can take and in which the occurrence of each value in between is equally probable.

**Sine distribution**

A distribution for which the relative number of occurrences of each of the possible angles between 0 and 180 degrees is proportional to the sine function.

**Cosine distribution**

A distribution for which the relative number of occurrences of each of the possible angles between 0 and 90 degrees is proportional to the cosine function.

more likely that cells will be observed in a random rather than a persistent migration mode. Thus, the turning angle frequency distribution will shift towards the (symmetrical) sine distribution (see Supplementary information S2 (figure) for an example from an experimental data set). This implies that a fair comparison of turning angles is possible only for experiments that are carried out at the same frame rate. The frame rate is a somewhat arbitrary choice because the turning of cells results from imaging a continuous cell path at discrete time points, but the time between frames should be kept well below the typical duration of persistent cell motion.

Another example of angle measurement is the angle between the direction of travel and the shortest route of a cell towards certain points of interest (FIG. 3c) (such as dendritic cells that might attract T cells through the production of chemokines). Plotting the mean (and standard error) of these angles as a function of the distance to those points of interest will show whether cells tend to be attracted towards those positions within the image volume, and how localized such directed migration is (FIG. 3d). For example, using such an angle analysis it was shown that naive CD8<sup>+</sup> T cells are attracted to sites of CD4<sup>+</sup> T cell–dendritic cell interactions<sup>21</sup>. A conventional mean

displacement plot cannot distinguish between migration affected by the presence of multiple local attractors and a ‘true’ random walk<sup>22</sup>. An additional important factor to consider in the study of directed migration in general is that it can be caused by mechanisms other than chemokine attraction. For example, anatomical constraints such as blood vessels or fibroblastic reticular cells may also influence cell migration<sup>23–25</sup>.

Angle measurements can be extremely powerful in detecting subtle phenomena. For example, we studied the angle between the directions of travel of T cells as a function of the distance between each other, both in space (at the same time point) and in time (at the same location)<sup>15</sup>. We found evidence for the presence of dynamic microstreams of naive T cells in lymph nodes. A factor that may obscure the detection of non-random migration angles is the pausing behaviour of cells, because pausing cells may have random migration angles. This problem can be solved by calculating migration angles for fast movement steps only. Because angle measurements can detect subtle migration effects, they are helpful for the detection and correction of artefacts (see below).

In summary, a powerful set of tools is available to analyse the motility of immune cells. These vary from qualitative track plots to more quantitative measures such as cell speed, motility coefficient, confinement ratio and turning angles. As discussed above, migration angles can be calculated that can help to answer questions such as whether immune cells are attracted by certain chemokines.

**Dealing with artefacts and biases**

It is well known that both the imaging of fluorescently labelled cells *in vivo* or in explanted tissue and the subsequent cell tracking to obtain three-dimensional coordinates of cells over the time course of an experiment can result in errors in the resulting data sets. Below we discuss several potential artefacts that are probably present in many experimental data sets, and we suggest ways to detect their presence and avoid or correct them in the data analysis.

**Artefacts of cell tracking.** Automated cell tracking is carried out with the aid of specialized software, and new tracking algorithms are continuously being designed<sup>26,27</sup>. It is well known that automated cell tracking rarely gives an error-free result, and manual corrections are therefore an essential subsequent step.

An obvious problem in cell tracking occurs when individual cells come into close contact with each other (FIG. 4a). When these cells are labelled with the same fluorescent marker, it can be difficult to identify which cell is which in the subsequent time frames, even for a human observer. Thus, automated tracking can easily result in the ‘switching’ of tracks (whereby two cells cross paths and are assigned the wrong path after the close apposition of their cell membranes). A possible solution is to use stringent algorithm settings such that different tracks are assigned to the cells before and after they approach each other closely. However, such ‘splitting’ of tracks obscures the long-term behaviour of a cell.

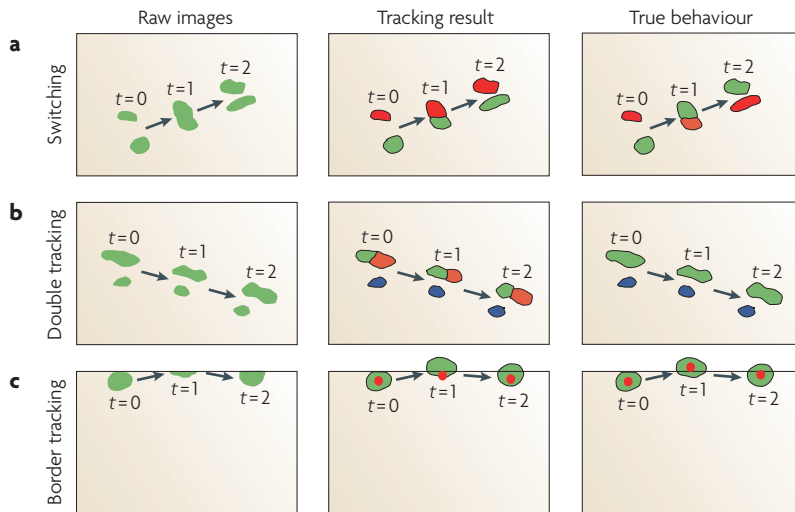


**Figure 4 | Scheme showing the artefacts in time-lapse imaging data that are due to tracking errors.** **a** | Switched tracks can occur when the cell membranes of two cells become closely apposed. **b** | A cell can be tracked twice if the tracking algorithm designates a large or stretched cell as two cells. **c** | Near the border of the image volume, it is difficult to estimate the centre of mass of cells (red dots are true or estimated centres of mass). Time steps are denoted by  $t$ .

Another type of error that might be introduced by automated cell tracking is that cells could be missed for a part of the period of imaging, or that cells could erroneously be tracked twice because the software may designate two cells to what is in reality a single large or stretched cell. This could even happen for several time frames in a row (FIG. 4b). Such double tracking is even more likely to occur when multiple fluorophores are used to label cells in the experiment: because of small overlaps in the emission spectra of different fluorescent markers, the software might track a single cell twice (in two colours).

We propose that the manual correction of both switching or splitting and double tracking could be optimized by the following approach: for all possible cell pairs, plot the angle between the directions in which each of the two cells of a pair are travelling versus the distance between the two cells (FIG. 5a). When the distance between cells is below a certain threshold value, these cells are in close proximity and this could be used to check the tracking in an organized and consistent manner for the occurrence of switching or splitting and double tracking. For double tracking, especially those cell pairs that travel in a similar direction are suspect.

Another potential tracking artefact is related to the fact that only a limited volume can be visualized during imaging experiments. Cells near the border of the image volume are hard to track because they might be in the process of leaving or entering that volume. As a consequence, it is difficult to determine the actual centre of mass of such cells (FIG. 4c). Cell positions estimated by tracking software are based on the voxels within the image volume, so this results in a centre of mass within that volume. Errors in calculating the centre of mass are most pronounced in the axial dimension (that is, the  $z$  axis direction) because of excitation of fluorophores outside the focal plane<sup>28</sup>. Such out-of-focus excitation means that even a

cell that is in reality completely outside the image volume could still give rise to excitation and thus be assigned a centre of mass inside the volume. This tracking artefact leads to cellular migration that seems to be parallel to the image borders. It also introduces errors in migration parameters, for example speed and displacement become underestimated at the image borders.

An approach that can help to detect border tracking errors is to study the angle between cell movements and the border planes as a function of the distance to the given plane. When migration seems to be parallel to the border for cells that are close to it (FIG. 5b), this is likely to be an artefact. To prevent such artefacts from affecting the analysis, we suggest that any cell movement that has a starting coordinate within a limited distance (this distance could be based on the above analysis) of one of the borders should be discarded. Note that the tracking itself should first be carried out for the entire image volume, and not for the smaller region with the borders stripped off.

**Imprecise  $z$  calibration.** Imaging experiments, whether they are carried out on explanted organs or *in vivo*, are complex to set up and perform, and the imaging itself could lead to artefacts in the observed behaviour<sup>29</sup>. For example, a well-known problem is that phototoxicity can give rise to anomalous cell motility. Another issue is that different  $x$  and  $y$  resolutions (typically 0.5–1  $\mu\text{m}$  steps) and  $z$  resolutions (typically 3–5  $\mu\text{m}$  steps) are generally used in experiments. Independent of the different resolutions, the determination of the exact spatial location of fluorophore excitation is fundamentally less precise in the axial than in the lateral dimensions<sup>28</sup>.

However, an even bigger and not so well-known problem is that the calibration of the voxel size in the axial dimension is imprecise. This can be shown by studying the projections of the velocity vectors of travelling cells in each of the three dimensions separately. For migration that is completely random in all directions, the cells and thus their velocity projections are expected to behave in the same way in each dimension. In experimental data sets of immune cell migration, this is typically true for the two lateral dimensions but not for the axial dimension — that is, the average velocity component in the  $z$  axis direction is generally different from that in the  $x$  and  $y$  axis directions. We compared data sets from various laboratories and found that the axial velocity components usually differ by 10–20% from the lateral velocity components (either slower or faster movement).

The reasons for the difficulty of  $z$  calibration are not entirely clear, but one factor is the refractive index of the investigated tissue and of the immersion fluid used. This index is difficult to determine for tissues but the estimated  $z$  axis positions (and thus the velocities) strongly depend on it. To obtain a more precise  $z$  calibration it would be helpful to use time-lapse imaging of cells in an environment where it is known that cells migrate randomly. For that purpose the migration of naive T cells within the lymph node paracortex in the absence of cognate antigen could be used, because it has been found that migration is essentially random in that case<sup>30</sup>.

#### Voxel

A volume element on a regular lattice in three-dimensional space.

#### Phototoxicity

Cell death and other artefactual cell behaviour associated with illumination during fluorescence microscopy.

#### Refractive index

A measure of how much the speed of light is reduced inside a medium, causing the light to change direction at the interface of two different media.

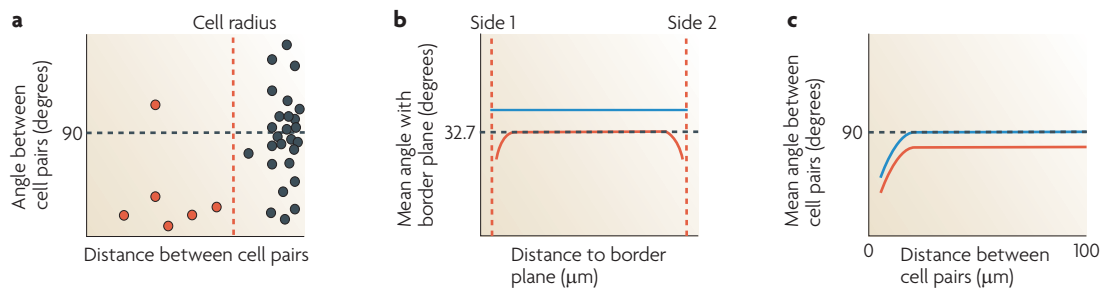


**Figure 5 | Using angle measurements to detect artefacts.** **a** | Plotting the angle between the directions of cell pairs as a function of the distance between them. Cell pairs may have been tracked twice when their centres of mass are extremely close (red dots), especially when the angle between their migration directions is low. Cells that are close together can also be used to assist in the detection of splitting or switching of tracks. The red dotted line indicates the typical radius of a cell. **b** | Plotting the mean angles with a border plane versus the distance to that plane can help to find deviations from expectation (black dotted line at  $\sim 32.7$  degrees) due to artefacts such as errors in tracking near borders (red solid line) or an imprecise  $z$  calibration (blue line). **c** | Plotting the average angle between the migration directions of cell pairs as a function of the distance between them (blue solid line gives expectation). Artefacts can influence the observed relationship, for example tissue drift leads to apparent large scale correlated movement (red line).

However, it is probable that the problem of the axial resolution cannot be entirely resolved by sufficiently precise calibration. Therefore, we propose a correction to the  $z$  axis coordinates for those data sets in which the difference between axial and lateral velocities is not known with certainty to be a real phenomenon. This correction can be made by multiplying each  $z$  axis coordinate by an appropriate factor such that the average velocity components in each dimension become equal.

**Small tissue drift.** Another artefact of time-lapse imaging that cannot be entirely avoided is the slow drifting of the entire imaged tissue. This obviously occurs in intravital imaging studies in which the anaesthetized animal is alive and therefore is making small movements. However, tissue drift also occurs in organ explant experiments, because the flow of medium causes slow drifting of the entire organ despite its firm attachment. The presence of such tissue drift means that the whole visualized volume, including all of the fluorescent cells within it, shifts slightly during the experiment (this is often visible in the videos). Frequently, tissue drift seems to be constant, but sometimes a clear change in the direction or speed of the flow is evident. When this drift is not corrected for, the cell movements that are analysed by tracking will contain an artefactual component that is caused by the movement of the entire field. Typically, the size of that artefactual component is of the order of tens of  $\mu\text{m}$  per hour, which is much slower than the average T cell migration speed of  $\sim 10 \mu\text{m}$  per minute in lymphoid tissues in the absence of cognate antigen<sup>2,30,31</sup>. Thus, small tissue drift has a limited effect on the average speed of immune cells. However, it may obstruct the detection of other migration phenomena such as directed migration. Furthermore, drift in the axial dimension might especially lead to misinterpretations because cells might seem to be dividing when they are not, or because the number of visible cells might dramatically change as the image volume drifts to another depth.

An approximate correction for tissue drift can be carried out if a static cell population (relative to the dynamic population under analysis) is visualized. Examples of such static cellular structures are blood vessels, the networks of fibroblastic reticular cells and follicular dendritic cells in lymph nodes<sup>23,32–35</sup>, or collagen fibres visualized by second harmonic generation. To use such cell populations for correction, it is important to detect multiple well-defined objects, for example certain cell bodies or parts of cells, that are entirely within the image volume over successive time-lapse images. The average displacement of the centres of mass of those objects can then be calculated for each time point, and that movement (which is thus assumed to be artefactual instead of real) can be subtracted from the movement of all tracked motile cells. Alternative options for tissue drift correction include the use of the displacement of the centres of mass of a subpopulation of fluorescently labelled cells that seem to be non-motile, the use of the mean displacement of the entire visualized cell population or the displacement of low-velocity movements only<sup>15</sup> (in the absence of chemokine gradients there might be no net displacement for the entire cell population, but obviously this cannot be used if the purpose of the experiment is to detect directed migration). When a large number of cells is imaged, this might give a reasonable correction.

To assist in the detection of and correction for tissue drift, it is helpful to plot the mean of the angles between the travel directions of all cell pairs as a function of the distance between the two cells of a pair (FIG. 5c). Cells that are located far apart should on average not show a directional preference if the migration is random. If such a preference is found, it can be indicative of motion biased in a certain direction, for instance as a result of a chemokine gradient, but it can also result from tissue drift. We recently used the cell-pair angle analysis to detect and correct for tissue drift<sup>15</sup>.

Studying migration angles relative to the border planes is also a helpful tool in the detection of both tissue drift and imprecise  $z$  calibration. For instance, if the axial velocity

#### Tissue drift

The artefactual movement of an entire specimen during an imaging experiment. It gives the impression that cells within the tissue are moving collectively in a certain direction.

#### Second harmonic generation

An optical process in which photons are formed that have twice the energy of the initial photons (and thus half of the original wavelength) when interacting with nonlinear materials such as collagens.

is higher than the lateral velocities owing to imprecise  $z$  calibration, this would result in an overall increased angle to the axial border plane (FIG. 5b, blue line). A similar effect would occur when there is a tissue drift component along the  $z$  axis. Examples of artefact detection and correction in experimental data sets using angle measurements are shown in [Supplementary information S3](#) (figure).

**Bias of cell-based parameters.** There are two slightly different ways to quantify cell migration parameters. Most researchers first carry out a calculation for each cell separately; from the results of those calculations, the mean or median for the entire population of cells is determined ('cell-based parameters'). Alternatively, the mean or median of all separate movement steps can be calculated independent of which track it belongs to ('step-based parameters').

An advantage of the cell-based approach is that it is more intuitive to think about the behaviour of single cells than that of the entire population. Furthermore, the visualized population could consist of subpopulations that have different, biologically relevant behaviours. This might be discovered by plotting the distribution of the parameter of interest among all cells or by studying correlations between multiple cell-based parameters. For example, cortical thymocytes were found to consist of a subpopulation of slow, randomly migrating cells and a subpopulation of fast-moving cells with a preferential movement perpendicular to the thymic capsule, and it was suggested that the fast-moving subpopulation might be positively selected thymocytes<sup>36</sup>. In a step-based approach, subpopulations might be overlooked. Sometimes, a cell-based approach is the only way to investigate the problem at hand, for example when the ancestors of dividing cells are traced.

However, cell-based parameters can be biased for multiple reasons. The most important reason is related to the fact that scanning of multiple  $z$  stacks takes time, and the investigator needs to find a compromise between the image volume size and the delay between sequential time frames. Typically, image volumes are wide in the lateral directions (hundreds of  $\mu\text{m}$ ) but narrow in the axial direction (usually around 40  $\mu\text{m}$ ). Because of the limited image volume, cells are continuously entering and leaving that space, especially in the axial dimension. Therefore, the time period during which cells are in view differs greatly between cells, and this could influence the value of the calculated parameter of that cell. For example, fast moving cells have a tendency to stay in the image volume for short periods of time (before leaving mainly in the axial dimension). Such cells are also likely to have relatively straight tracks (as they have a high confinement ratio and low turning angles) and thus might seem to be a separate subpopulation. However, if these cells could be followed for longer periods of time they might in fact not be moving so fast and straight. So, the shape of the visualized space affects the type of motion that is preferentially detected by cell-based parameters. This also means that a change in the volume or shape of the imaged space influences the calculated parameters, which might be one of the factors

explaining the variability between results from different laboratories. Frequently, researchers require tracks to be in view for several minutes to be included in their analysis, which introduces another bias towards more slowly moving cells. Another reason for the presence of biases in cell-based parameters is the discussed artefacts. For example, splitting of tracks causes a single cell to contribute multiple times to a cell-based parameter (note that the re-entry of cells to the image volume has a similar effect), and tracking errors near borders of the image volume would affect cell-based motility parameters.

These problems are largely resolved by using step-based rather than cell-based parameters. Movement steps that start near borders can be excluded from the calculations. The splitting of tracks and the re-entry of cells as new tracks are not major problems because for a step-based parameter it does not matter to which cell a movement step belongs. Even switching of tracks introduces only a limited error because only the few time steps involved in a switch are affected, rather than the entire track as would be the case for a cell-based parameter (note that in cases in which there is doubt, splitting of tracks is preferable to switching of tracks to avoid this limited error). Finally, the shape of the imaged space has little effect on step-based parameters because each individual movement step occurs within a very small part of the space. Only the steps that are near one of the borders could be biased, because detection is limited to movements that remain in view. Because steps that start near borders need to be removed anyway (to avoid tracking errors), this problem is automatically avoided.

Cell migration parameters, such as speeds and angle measurements, can easily be calculated in a step-based manner. However, for the mean displacement plot and the confinement ratio the biases associated with a cell-based approach cannot be easily avoided. Cells that are in view for a long time period tend to be cells that move slowly and have limited displacement (because faster moving cells with greater displacement are more likely to leave the image volume), which could lead to an underestimate of the mean displacement for large time steps and therefore to an apparent confinement of cells. Hence, using just the mean displacement plot, it may be difficult to distinguish between the possible types of migration behaviour (random, directed or confined migration). Similarly, the confinement ratio is a cell-based and thus biased approach. For example, among cells with long tracks, confined cells are over-represented because these tend to be the cells that stay within the image volume for long periods. To solve these issues, a reasonable step-based alternative to the confinement ratio is to calculate turning-angle distributions (see above). The mean displacement plot to detect migration processes that differ from a random walk can be complemented by studying other local angles of movement.

In conclusion, various artefacts related to time-lapse imaging (imprecise  $z$  calibration and small tissue drift) and to cell tracking (switching or splitting of tracks, double tracking and border tracking) are inevitably present in experimental data sets. However, a toolbox consisting

Table 1 | **Potential biases and artefacts in time-lapse imaging data, and tools for correction**

Artefact or bias	How to detect	How to correct
Switching and splitting of tracks	Two cells in close proximity are suspect (especially when the turning angles of both cells are large).	Manually study suspect cases and correct (in cases of doubt prefer splitting over switching).
Double tracking	Cell pairs in close proximity with similar travel directions are suspect.	Manually study suspect cases and correct where necessary.
Errors of tracking near borders	Plot the average angle to border planes as a function of the distance to those planes (visible as lower average angles near the borders).	Discard movement steps close to the border.
Imprecise z calibration	Plot the average angle to border planes as a function of the distance to those planes (visible as an average angle that is distinct from 32.7 degrees at any distance) or measure the velocity projections in each dimension separately.	Multiply each z axis coordinate with a factor such that the average velocity projections in each dimension become equal.
Small tissue drift	If cells that are distant from each other travel in similar directions, this may be indicative of tissue drift. Tissue drift will also affect the average angle of a cell to the border planes.	Subtract the average displacement of static cell populations or that of (low-velocity steps) of motile cell populations.
Cell-based parameters are biased	Not applicable.	Use step-based calculations whenever the scientific question allows. As an alternative for the confinement ratio, the straightness of tracks can be quantified by measuring turning angles. The mean displacement plot can be complemented by studying other migration angles.
The initiation or termination of contacts is not observed	Not applicable.	Estimate the true contact time distribution from the observed contact times <sup>40</sup> . The mean contact time can also be estimated using a straightforward rule <sup>40</sup> .

mostly of various angle measurements can help to detect and correct for such artefacts (TABLE 1). Furthermore, by using step-based rather than cell-based analysis methods most biases can be avoided.

### Contact time analysis

In addition to analysing immune cell migration, a frequently investigated parameter is the duration of interactions between immune cells (recently reviewed in REF. 37). Ideally, contact durations in different experimental conditions are compared and correlated to functional readouts of an immune response. For example, it was shown that the antigen dose sensed by T cells determines the duration of the phase of brief T cell–dendritic cell interactions, and that this correlates with T cell proliferation and effector function<sup>38</sup>. Unfortunately, contact duration, or the distribution of contact times, is a difficult parameter to determine because imaging is limited in both time and space. This means that for many contacts the initiation and/or the termination is not observed, and that the observed contact duration often underestimates the true duration.

Researchers usually calculate the mean or median of all the observed durations in an experiment, thus obtaining an underestimate of the true contact duration. Sometimes a distinction is made between contacts for which the exact duration is known and those for which it is not<sup>6,39</sup>. One strategy to try to find the true contact durations is to leave out those interactions for which the exact duration is not known<sup>5</sup>, but this introduces a

strong bias for brief interactions<sup>20</sup>. We recently developed a method to estimate the true contact time distribution by deriving the theoretically expected relationship between true and underestimated contact time<sup>40</sup>. An optimization algorithm can then be used to estimate the true contact time distribution from the underestimated contact times. Alternatively, an estimate for the mean true contact time can be obtained by using a straightforward ‘shortcut’ approach that is based on the average number of conjugates present and on the number of initiating, as well as terminating, contacts during the imaging period<sup>40</sup>. We are not aware of other approaches to estimate the true contact time distribution directly from contact time data.

Most of the discussed artefacts do not affect the observed contact durations. However, the artefact of tissue drift can have a strong impact on the duration of observed interactions, because it leads to conjugates moving in and out of view. This occurs mostly in the z axis direction because of the thin z stack that is normally used (for example, tissue drift of tens of  $\mu\text{m}$  per hour in combination with a 40  $\mu\text{m}$  z stack results in a large fraction of conjugates entering and exiting in a 1 hour experiment). In future experiments that aim to determine contact times, the effect of tissue drift can be minimized by increasing the image volume in the z axis direction (for examples see REFS 6 and 41) because on average conjugates will be further away from the borders. Imaging a more cube-like volume is therefore an important step to obtain reliable contact data results.

**Optimization algorithm**  
A numerical method for finding the values of a set of parameters such that the value of a function of those parameters is as small or large as possible. In a data-fitting procedure those parameter values represent the best fit.

### Box 1 | Optimization of experimental setup

To allow robust and powerful data analysis, an experimental design that includes the following considerations is important (see REFS 29 and 43 for a more detailed discussion of some of these issues):

- Choose the fluorescent labels such that overlap of the fluorophore emission spectra is minimized.
- The cell number needs to be sufficiently high to generate enough data points in one image sequence, but not too high as this makes tracking problematic.
- The fluorescence intensity of the cells needs to be sufficient to find which voxels belong to cells, but it should not lead to saturated images.
- Minimize phototoxicity, thermal damage and toxicity due to the dye used.
- Choose an image acquisition speed and image volume size that can capture the behaviour of interest. We recommend an axial dimension (along the z axis) higher than is typical of current practice (especially for contact time measurements) because this helps to avoid biases caused by cell-based analysis. However, it should be noted that there is a compromise between image volume size and the spatial and temporal resolutions of the images.
- Aim for imaging of a control population of cells in the same experiment, as this helps to obtain a fair comparison of the behaviour of different cell types.
- Calibrate the spatial dimensions (especially the axial dimension) for the imaged tissue as well as possible, preferably by using a control population of cells that is expected to migrate randomly.
- During experiments, try to keep tissue drift as small as possible, especially in the axial dimension.

### Concluding remarks

Here, we have proposed ways in which the analysis of time-lapse microscopy data on migration of and interactions between cells of the immune system can be refined. We have discussed various artefacts that are present in many cell migration data sets and how these issues can be resolved (TABLE 1). Some of these approaches can also assist in the manual correction of automated tracking results by identifying the parts of tracks to be checked for correctness. We have emphasized that data analysis can lead to biased results and because the shape and size of the imaged

space influences cell-based calculations we propose that step-based methods should be used whenever the question of interest allows this. A further improvement in that respect would be to make the image volume used more equal in size in each dimension than is the current experimental practice (see BOX 1 for further experimental setup considerations).

Depending on the scientific questions asked and the amount of detail needed for the answer, the discussed artefacts and biases could have a limited or a large effect on the quantitative results and their interpretation. For example, small tissue drift will minimally affect the average speed of immune cells, but it may have a strong effect on the measurement of directed migration and on estimated contact times between cells. The importance of artefact correction further depends on the size of the differences between experimental settings: when small but biologically relevant differences are present, they may be obscured by artefacts and thus be missed in the analysis. By contrast, artefacts or biased analysis may produce spurious results in the form of small differences that are not really there between experimental settings. In general it is important to correct for artefacts because subtle differences in cell migration behaviour may have important functional consequences on the level of the entire immune system. For example, subtle chemokine-mediated attraction of naive CD8<sup>+</sup> T cells to specific dendritic cells promotes memory CD8<sup>+</sup> T cell generation<sup>21</sup>. The toolbox that we propose here will further improve the comparability between experiments from different laboratories and is in general an important step towards a more quantitative analysis of imaging experiments. Although we have focused on approaches in the field of immunology, we expect that the issues discussed here will have a role in any scientific discipline investigating motility and interactions at the level of single cells, for example in imaging of development<sup>42</sup>.

- Bousoo, P., Bhakta, N. R., Lewis, R. S. & Robey, E. Dynamics of thymocyte-stromal cell interactions visualized by two-photon microscopy. *Science* **296**, 1876–1880 (2002).
- Miller, M. J., Wei, S. H., Parker, I. & Cahalan, M. D. Two-photon imaging of lymphocyte motility and antigen response in intact lymph node. *Science* **296**, 1869–1873 (2002).
- Stoll, S., Delon, J., Brötz, T. N. & Germain, R. N. Dynamic imaging of T cell-dendritic cell interactions in lymph nodes. *Science* **296**, 1873–1876 (2002).
- Lindquist, R. L. *et al.* Visualizing dendritic cell networks *in vivo*. *Nature Immunol.* **5**, 1243–1250 (2004).
- Mempel, T. R., Henrickson, S. E. & von Andrian, U. H. T cell priming by dendritic cells in lymph nodes occurs in three distinct phases. *Nature* **427**, 154–159 (2004).
- Allen, C. D., Okada, T., Tang, H. L. & Cyster, J. G. Imaging of germinal center selection events during affinity maturation. *Science* **315**, 528–531 (2007).
- Qi, H., Cannons, J. L., Klauschen, F., Schwartzberg, P. L. & Germain, R. N. SAP-controlled T–B cell interactions underlie germinal centre formation. *Nature* **455**, 764–769 (2008).
- Miller, M. J., Sadrina, O., Parker, I. & Cahalan, M. D. Imaging the single cell dynamics of CD4<sup>+</sup> T cell activation by dendritic cells in lymph nodes. *J. Exp. Med.* **200**, 847–856 (2004).
- Sumen, C., Mempel, T. R., Mazo, I. B. & von Andrian, U. H. Intravital microscopy: visualizing immunity in context. *Immunity* **21**, 315–329 (2004).
- Beauchemin, C., Dixit, N. M. & Perelson, A. S. Characterizing T cell movement within lymph nodes in the absence of antigen. *J. Immunol.* **178**, 5505–5512 (2007).
- le Borgne, M. *et al.* The impact of negative selection on thymocyte migration in the medulla. *Nature Immunol.* **10**, 823–830 (2009).
- Doi, M. & Edwards, S. F. *The Theory of Polymer Dynamics* (Clarendon, Oxford, UK, 1986).
- Rubinstein, M. & Colby, R. H. *Polymer Physics* (Oxford Univ. Press, New York, 2003).
- Wieser, S. & Schütz, G. J. Tracking single molecules in the live cell plasma membrane — do's and don'ts. *Methods* **46**, 131–140 (2008).
- Beltman, J. B., Marée, A. F. M., Lynch, J. N., Miller, M. J. & de Boer, R. J. Lymph node topology dictates T cell migration behaviour. *J. Exp. Med.* **204**, 771–780 (2007).
- Benhamou, S. How to reliably estimate the tortuosity of an animal's path: straightness, sinuosity, or fractal dimension? *J. Theor. Biol.* **229**, 209–220 (2004).
- Bogle, G. & Dunbar, P. R. Simulating T-cell motility in the lymph node paracortex with a packed lattice geometry. *Immunol. Cell Biol.* **86**, 676–687 (2008).
- Mrass, P. *et al.* CD44 mediates successful interstitial navigation by killer T cells and enables efficient antitumor immunity. *Immunity* **29**, 971–985 (2008).
- Preston, S. P., Waters, S. L., Jensen, O. E., Heaton, P. R. & Pritchard, D. I. T-cell motility in the early stages of the immune response modeled as a random walk amongst targets. *Phys. Rev. E Stat. Nonlin. Soft Matter Phys.* **74**, 011910 (2006).
- Beltman, J. B., Marée, A. F. M. & de Boer, R. J. Spatial modelling of brief and long interactions between T cells and dendritic cells. *Immunol. Cell Biol.* **85**, 306–314 (2007).
- Castellino, F. *et al.* Chemokines enhance immunity by guiding naive CD8<sup>+</sup> T cells to sites of CD4<sup>+</sup> T cell-dendritic cell interaction. *Nature* **440**, 890–895 (2006). **This report is an example of how migration angles can be used to find evidence for directed migration: sites of CD4<sup>+</sup> T cell-dendritic cell interaction were found to attract naive CD8<sup>+</sup> T cells by chemokines.**
- Germain, R. N. *et al.* An extended vision for dynamic high-resolution intravital immune imaging. *Semin. Immunol.* **17**, 431–441 (2005).
- Bajénoff, M. *et al.* Stromal cell networks regulate lymphocyte entry, migration, and territoriality in lymph nodes. *Immunity* **25**, 989–1001 (2006).
- Bajénoff, M., Glaichenhaus, N. & Germain, R. N. Fibroblastic reticular cells guide T lymphocyte entry into and migration within the splenic T cell zone. *J. Immunol.* **181**, 3947–3954 (2008).

25. Mueller, S. N. & Germain, R. N. Stromal cell contributions to the homeostasis and functionality of the immune system. *Nature Rev. Immunol.* **9**, 618–629 (2009).
26. Sergé, A., Bertaux, N., Rigneault, H. & Marguet, D. Dynamic multiple-target tracing to probe spatiotemporal cartography of cell membranes. *Nature Methods* **5**, 687–694 (2008).
27. Jaqaman, K. *et al.* Robust single-particle tracking in live-cell time-lapse sequences. *Nature Methods* **5**, 695–702 (2008).
28. Wei, S. H., Parker, I., Miller, M. J. & Cahalan, M. D. A stochastic view of lymphocyte motility and trafficking within the lymph node. *Immunol. Rev.* **195**, 136–159 (2003).
29. Germain, R. N., Miller, M. J., Dustin, M. L. & Nussenzweig, M. C. Dynamic imaging of the immune system: progress, pitfalls and promise. *Nature Rev. Immunol.* **6**, 497–507 (2006).
- This report provides an overview of technical issues related to dynamic imaging experiments, such as different fluorescent labelling methods and a comparison between intravital and explant experiments.**
30. Miller, M. J., Wei, S. H., Cahalan, M. D. & Parker, I. Autonomous T cell trafficking examined *in vivo* with intravital two-photon microscopy. *Proc. Natl Acad. Sci. USA* **100**, 2604–2609 (2003).
31. Bousso, P. & Robey, E. Dynamics of CD8<sup>+</sup> T cell priming by dendritic cells in intact lymph nodes. *Nature Immunol.* **4**, 579–585 (2003).
32. Gretz, J. E., Anderson, A. O. & Shaw, S. Cords, channels, corridors and conduits: critical architectural elements facilitating cell interactions in the lymph node cortex. *Immunol. Rev.* **156**, 11–24 (1997).
33. Gretz, J. E., Norbury, C. C., Anderson, A. O., Proudfoot, A. E. & Shaw, S. Lymph-borne chemokines and other low molecular weight molecules reach high endothelial venules via specialized conduits while a functional barrier limits access to the lymphocyte microenvironments in lymph node cortex. *J. Exp. Med.* **192**, 1425–1440 (2000).
34. Sixt, M. *et al.* The conduit system transports soluble antigens from the afferent lymph to resident dendritic cells in the T cell area of the lymph node. *Immunity* **22**, 19–29 (2005).
35. Allen, C. D. & Cyster, J. G. Follicular dendritic cell networks of primary follicles and germinal centers: phenotype and function. *Semin. Immunol.* **20**, 14–25 (2008).
36. Witt, C. M., Raychaudhuri, S., Schaefer, B., Chakraborty, A. K. & Robey, E. A. Directed migration of positively selected thymocytes visualized in real time. *PLoS Biol.* **3**, 1062–1069 (2005).
37. Davis, D. M. Mechanisms and functions for the duration of intercellular contacts made by lymphocytes. *Nature Rev. Immunol.* **9**, 543–555 (2009).
38. Henrickson, S. *et al.* T cell sensing of antigen dose governs interactive behavior with dendritic cells and sets a threshold for T cell activation. *Nature Immunol.* **9**, 282–291 (2008).
39. Mrass, P. *et al.* Random migration precedes stable target cell interactions of tumor-infiltrating T cells. *J. Exp. Med.* **203**, 2749–2761 (2006).
40. Beltman, J. B., Henrickson, S. E., Von Andrian, U. H., De Boer, R. J. & Marée, A. F. M. Towards estimating the true duration of dendritic cell interactions with T cells. *J. Immunol. Methods* **347**, 54–69 (2009).
- This report presents a computational method to estimate the true rather than the underestimated distribution of contact times between cells using a mathematical approach.**
41. Gardner, J. M. *et al.* Deletional tolerance mediated by extrathymic Aire-expressing cells. *Science* **321**, 843–847 (2008).
42. Keller, P. J., Schmidt, A. D., Wittbrodt, J. & Stelzer, E. H. Reconstruction of zebrafish early embryonic development by scanned light sheet microscopy. *Science* **322**, 1065–1069 (2008).
43. Waters, J. C. Accuracy and precision in quantitative fluorescence microscopy. *J. Cell Biol.* **185**, 1135–1148 (2009).

### Acknowledgements

We would like to thank C. Allen, U. von Andrian, S. Ariotti, J. Cyster, S. Henrickson, J. Lynch, T. Mempel, M. Miller and T. Schumacher for discussing various aspects of cell migration and cellular interactions, and M. Miller for letting us use previously published data from his group to illustrate some of the issues discussed. This work was supported by the Netherlands Organization for Scientific Research (NWO), grants 916.86.080 (J.B.B) and 016.048.603 (R.J.d.B).

### FURTHER INFORMATION

Joost B. Beltman's homepage: <http://theory.bio.uu.nl/joost>

### SUPPLEMENTARY INFORMATION

See online article: [S1](#) (box) | [S2](#) (figure) | [S3](#) (figure)

ALL LINKS ARE ACTIVE IN THE ONLINE PDF